ISBN: 978-3-95450-132-8 doi:10.18429/JACoW-IPAC2014-THPME196

LOW ENERGY CODED APERTURE PERFORMANCE AT THE CESR-TA X-RAY BEAM SIZE MONITOR*

J. P. Alexander, A. Chatterjee, M. P. Ehrlichman, B. K. Heltsley, A. Lyndaker, D. P. Peterson, N. T. Rider, D. Rubin, R. Seeley, J. Shanks, Cornell University, Ithaca, NY 14853, USA
J. Flanagan, High Energy Accelerator Research Organization (KEK), Tsukuba, Japan

Abstract

We report on the design and performance of coded aperture optics elements in the CESR-TA x-ray beam size monitor (xBSM). Resolution must be sufficient to allow single-turn measurements of vertical beam sizes of order 10 µm by imaging synchrotron radiation photons onto a one-dimensional photodiode array. Measurements with beam energies above 2.1 GeV and current above 0.1 mA can be performed with a single-slit (pinhole) optic. At lower energy or current, small beam size measurements are limited by the diffractive width of a pinhole image and counting statistics. A coded aperture is a multi-slit mask that can improve on the resolution of a pinhole in two ways: higher average transparency improves counting statistics; and the slit pattern and masking transparency can be designed to obtain a diffractive image with narrower features. We have previously implemented coded apertures that are uniform redundant arrays (URA). A new coded aperture design is optimized for imaging with 1.8 GeV beam energy (1.9 keV average x-ray energy) and with beam sizes below 20 µm. Resolution measurements were made in December 2013. Performance of the new coded aperture is compared to the pinhole and the URA.

INTRODUCTION

Precision measurement of vertical bunch size plays an increasingly important role in the design and operation of the current and future generation of electron storage rings. By providing the real-time vertical beam size information, the accelerator can be tuned in a predictable, stable, and robust manner. Challenges persist in obtaining precision at low beam size and current. We have previously described [1-7] the CESR-TA x-ray beam size monitor (xBSM), which images synchrotron radiation from a hard-bend magnet through an optical element onto a 32-strip photodiode detector with 50 µm pitch and fast readout. Here we extend the characterization of that device, focusing on comparing measured resolving power for several different optical elements with that predicted for each from simple models. Optical elements include both single-slit (pinhole) and multi-slit patterns, the latter of which are known as coded apertures.

*Work supported by National Science Foundation awards PHY-0734867, PHY-1002467, PHYS-1068662, and Department of Energy contracts DE-FC02-08ER41538 and DE-SC0006505, and by the NSF and National Institutes of Health/National Institute of General Medical Sciences under NSF award DMR-0936384.

Separate installations of the CESR-TA xBSM exist for electrons and positrons. The optical element is placed at 4366 (4485) mm from the x-ray source point and the detector is placed 11621 (10012) mm from the optical element in the electron (positron) installation; the magnification is 2.438 (2.232). X-rays are horizontally collimated at the optical elements with a window of 0.5 mm for the pinhole and 1.1 mm for the coded apertures. The detector is 0.4 mm wide in the horizontal; the collimation does not shadow the detector but careful alignment is required.

UNIFORMLY REDUNDANT ARRAYS

Coded aperture imaging is a technique well developed among x-ray astronomers [8] which can, due to greater x-ray collection efficiency, improve on the spatial resolution of a pinhole camera. A coded aperture has multiple light transmitting elements and the image is a complicated superposition of the images from each transmitting element. Thus, the image, I, can be described by

$$I = O \times A + N, \tag{1}$$

where O is the object, A is the aperture and describes the transfer of light from each position of the object to the image, and N is a description of detector noise. While the object is typically 2-dimensional in astronomy applications, the CESR-TA xBSM is a 1-dimensional device. The aperture in Eq. 1 is then a square matrix in which each column describes the point response function (PRF) at the detector for light originating from an array of (digitized) light source locations in the object.

A Uniformly Redundant Array (URA) [9] is a coded aperture optimized to minimize the effect of noise on the computed object. In a 1-dimensional URA, features are described by a series of equal-size cells that are either transmitting or opaque. Features of the optical element are made up of one or more contiguous same-transmission cells. The redundancy is a measure of the number of times that pairs of transmitting cells are separated by a particular distance. In a URA, the number of times that each separation is observed is uniform regardless of separation (up to a limit due to the finite array length).

Our starting point for coded aperture studies [7, 10-13], is a 31 cell URA with the pattern,

URA (31)=0110110111100010101110000100100

ISBN: 978-3-95450-132-8 doi:10.18429/JACoW-IPAC2014-THPME196

where transmitting (opaque) cells are represented by 1(0). This pattern has a nearly uniform redundancy of about 6, up to a cell separation of 10. Figure 1 shows the PRF for the URA, with opaque mask material and without the effects of diffraction, on a hypothetical 128 channel detector.

With a URA, even a multi-point object can be reconstructed by applying a processing array, G:

$$O' = I \times G = O \times (A \times G) + N \times G. \qquad (2)$$

Note that G is not A^{-1} as might be expected. A^{-1} may have large elements causing an amplification of detector noise through the term: $N \times A^{-1}$. Instead, with uniform redundancy, the autocorrelation matrix $A \times A$ is small unless $i=j$. G is constructed by applying a baseline shift to A; $G_{ij}=2(A_{ij}-0.5)$. The product, $A \times G$, shown in Fig. 1, has a central peak indicating that the object will be reconstructed. The reconstructed object has limited noise due to $N \times G$ and the background in $A \times G$.

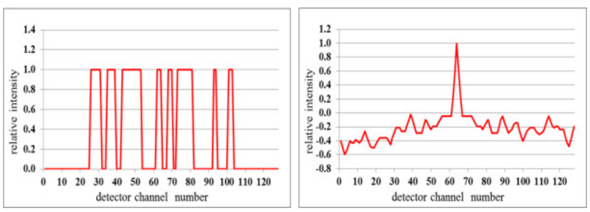

Figure 1: PRF (left) and product, A x G (central column), for URA (31) with no diffraction and opaque masking.

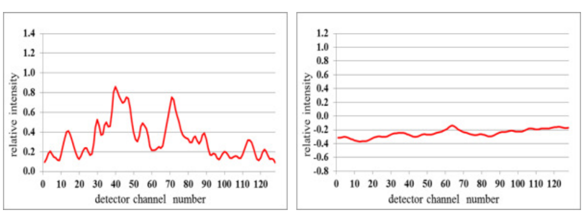

Figure 2: PRF (left) and A x G for URA (31) with the predicted x-ray energy spectrum and 0.60 μm Au masking. The area of this PRF is the same as in Fig. 1.

A URA is effective because A x G approximates a delta function. However, the use of semi-transmitting mask material and the effects of diffraction compromise the effectiveness of the URA. Figure 2 shows the PRF and product, A x G, of the same URA with the CESR-TA x-ray energy spectrum and 0.60 μm gold mask material. The effects on the PRF are to wash out the sharp edges and introduce diffractive structure. The central peak in A x G is now barely discernable. However, there are still benefits in the URA due to the increased x-ray collection efficiency.

In the case of the xBSM, the object is a single source with Gaussian vertical spread. Therefore, instead of Eq. 2, we are able to reconstruct the object by applying a fitting method to a coded aperture image with knowledge of the PRF [7].

OPTIMUM INTERFERENCE APERTURE

We have taken an alternative approach to designing a coded aperture that exploits interference effects to optimize the resolving power. A feature of our coded apertures is that the thin mask material partially transmits x-rays with a phase shift. Thus, the PRF will depend on the x-ray spectrum, slit and mask sizes, and the mask transparency and phase shift.

We form a χ^2-like figure of merit, Q, for the beam-size resolving power based on the assertion that the pulse height in each of the 32 pixels is proportional to the number of absorbed x-ray photons and will fluctuate according to counting statistics [7]. In a simplified form, Q is defined, for a given vertical beam size, σ_b, by

$$Q(\sigma_b) = Q_0(\sigma_b/\delta)^2 \times \sum_{\text{pixels}} \frac{[P_j(\sigma_b) - P_j(\sigma_b+\delta)]^2}{P_j(\sigma_b) + P_j(\sigma_b+\delta)} \;, \qquad (3)$$

where Q_0 is a normalization factor, δ is an incremental change in the beam size, and $P_j(\sigma)$ is the PRF convolved with a Gaussian beam shape for detector pixel j. The optimal coded aperture design maximizes Q, thus maximizing the sensitivity of a fit to an image to variations σ_b. We have studied Q for various apertures including the URA described above, single slits, gratings, and the design described below.

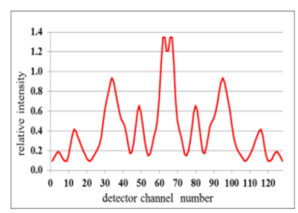

Figure 3: PRF for the interference optimized aperture (OIA), using the predicted x-ray energy spectrum.

The optimized interference aperture (OIA) was determined by evaluating Q for candidates in an iterative ad-hoc method and maximizing Q over the relevant beam size range. The features are not constrained to be built from equal size cells as in the case of the URA. The resulting coded aperture is symmetric with 5 slits in the pattern: 24S-10M-38S-42M-68S-42M-38S-10M-24S, where slits are designated "S" and mask material "M", and the numbers denote the vertical size of the elements in μm. For comparison, the URA used in these measurements was fabricated with a cell size of 10 μm resulting in an 8-slit pattern: 20S-10M-20S-10M-40S-30M-10S-10M-10S-10M-30S-40M-10S-20M-10S.

OPTICAL ELEMENTS STUDIED

Our coded apertures were acquired from Applied Nanotools, Inc. [14], and are etched with a proprietary process into a thin gold layer on a 2.5 μm-thick silicon substrate chip. The designs used in this study, URA and OIA, appear in high resolution photographs in Fig. 4. Optical measurements indicate that the systematic

ISBN: 978-3-95450-132-8 doi:10.18429/JACoW-IPAC2014-THPME196

placement of features is within 0.5 μm of the specifications. Edge quality is better than 0.1 μm rms deviation. One chip used in this study had both an OIA and URA with gold thickness 0.60 μm. Another chip provided a second URA with gold thickness 0.71 μm.

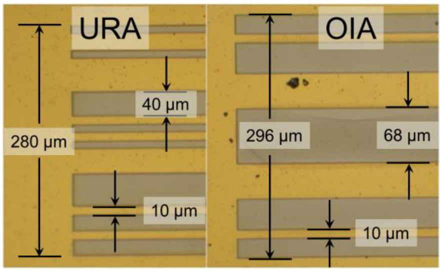

Figure 4: Microphotographs of the coded apertures. The masking material is 0.60 μm gold.

A 1-dimensional pinhole, or single slit, is also used in this study for comparison. The pinhole is formed between two thick tungsten masks [7], with a nominal opening of 50 μm.

MEASUREMENTS

To extract a measured resolving power from the data that can be compared to the prediction, we replace σ_b in Eq. 3 with $<\sigma_b>$, the turn-averaged measured beam size, and δ^2 with $<(\Delta\sigma_b)^2>$, the variance. The summation term is then the $\chi 2$ change of a fit to the beam size at the variance and is unity. Thus, Eq. 3 is rearranged to

$$Q(\sigma_b) = 0.01\mathrm{mA}/I_b \ <\sigma_b>^2 / <(\Delta\sigma_b)^2> \quad (4)$$

where Q_0 has been defined to yield a value of $Q(\sigma_b)=1$ for the smallest beam current of interest, 0.1 mA, and a marginal measurement of ~3σ separation from zero. Equation 4 represents the resolving power in an ideal experiment. In practice, measurements are taken at different currents, affecting the counting statistics of low-illumination regions of the detector. (This is particularly an issue in the case of the pinhole optic.) In addition, experimental horizontal misalignment can result in a less than full illumination of the detector. To correct for these effects, the predicted resolving power is recalculated from a simulation of the data taking into account Poisson photon-counting statistics, digitization, the discrete pixel size of the detector, individual channel pedestal fluctuations, and random flat background fluctuations. The measured resolving power is scaled by the ratio the predicted resolving power calculated with as-measured beam current and horizontal illumination to predicted resolving power calculated with fixed reference values.

Measurements of the resolving power as a function of beam size were made in December 2013 with 2.1 GeV electrons. Results are shown with the predicted resolving power in Fig. 5. Agreement between measured and predicted resolving power for all optical elements is reasonably good. The data confirms the prediction that the OIA outperforms the URA and the pinhole for beam sizes between 10 and 50 μm. The key to the effectiveness of the OIA is that the slits are spaced closely enough for diffraction to sharpen the primary peaks in the image but far enough away that the primary peaks do not merge together until a beam size of about 60 μm.

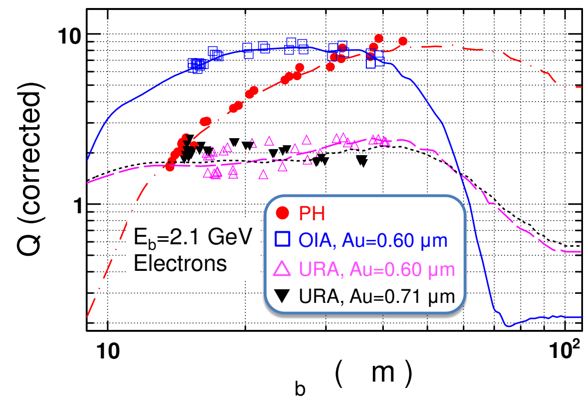

Figure 5: Resolving power: predicted (curves) and measured (points) for 2.1 GeV beam energy.

CONCLUSION

The results verify that the tools are effective for designing coded apertures for specific current and beam size regimes. At a beam size of 10 μm, beam current of 0.1 mA, and beam energy of 2.1 GeV, the Q for the OIA indicates that single turn measurements can be made with $\Delta\sigma_b/\sigma_b \approx 0.2$ and that with beam energy 1.8 GeV, single turn measurements can be made with $\Delta\sigma_b/\sigma_b \approx 0.3$ [7].

ACKNOWLEDGMENT

We acknowledge the efforts of the CESR Operations Group as well as the support of the Cornell Laboratory for Accelerator-based Sciences and Education (CLASSE) and Cornell High Energy Synchrotron Source (CHESS).

REFERENCES

[1] J. P. Alexander *et al.*, PAC09-TH5RFP026.
[2] J. P. Alexander et al., PAC09-TH5RFP027.
[3] D. P. Peterson et al., IPAC10-MOPE090.
[4] N.T. Rider et al., PAC11-MOP304.
[5] N. T. Rider et al., IBIC12-WEDC01.
[6] J. P. Alexander, D. P. Peterson, Handbook of Accelerator Physics and Engineering, 2nd Ed., Edited by A.W. Chao, K. H. Mess, M. Tigner, F. Zimmerman, (World Scientific, Singapore, 2013) p.721.
[7] J. P. Alexander *et al*, Nucl. Inst. and Meth. In Physics Research A 748, 96-125 (2014).
[8] R. H. Dicke, Astrophys. Journ. 153, L101 (1968).
[9] E. E. Fenimore and T. M. Cannon, Applied Optics vol. 17, No. 3, 337 (1978).
[10] J. W. Flanagan et al., EPAC08-TUOCM02.
[11] J. W. Flanagan et al., PAC09-TH5RFP048.
[12] J. W. Flanagan et al., IPAC10-MOPE007.
[13] J. W. Flanagan et al., DIPAC11-WEOB03.
[14] Applied NanoTools, Inc. #1200 - 10045 111 Street, Edmonton, Alberta T5K 2M5, CANADA.